# Spontaneously Forming Ellipsoidal Phospholipid Unilamellar Vesicles and Their Interactions with Helical Domains of Saposin C

Mu-Ping Nieh,*,† Jeremy Pencer,† John Katsaras,†,‡ and Xiaoyang Qi§

*Canadian Neutron Beam Center, Steacie Institute for Molecular Sciences, National Research Council at Canada, Chalk River, Ontario, Canada K0J-1J0, Guelph-Waterloo Physics Institute and Biophysics Interdepartmental Group, Guelph, Ontario, Canada, and Division of Human Genetics, Cincinnati Children Hospital Medical Center and University of Cincinnati College of Medicine, Cincinnati, Ohio 45229*

We have observed a bimodal distribution of ellipsoidal unilamellar vesicles (ULVs) in a phospholipid mixture composed of dioleoyl phosphatidylserine (DOPS) and dipalmitoyl and dihexanoyl phosphatidylcholine, DPPC and DHPC, respectively. Dynamic light scattering and transmission electron microscopy data indicate a bimodal size distribution of these nanoparticles with hydrodynamic radii of ~200 and >500 nm, while small-angle neutron scattering data were fit using a model of coexisting monodisperse morphologies, namely, oblate and triaxial ellipsoidal vesicles. Unlike DOPS ULV formed by sonication, which can fuse days after being formed, these ULVs are stable over a period of 12 months at 4 °C. We also report on the structure of these ULVs associated with the two helical peptide domains (H1 and H2) of a glucosylprotein, namely, Saposin C, to gain some insight into protein–membrane interactions.

## Introduction

Low polydispersity, spontaneously forming unilamellar vesicles (ULVs) can be found in the phase diagram of ternary phospholipid mixtures containing long and short acyl chains.[1-3] The ULVs are formed either by increasing the temperature[4,5] or diluting bilayered discoidal micelles[2] where the short-chain lipid sequesters into the high-curvature rim of the bilayered disk, minimizing its edge energy. The discoidal bilayered micelle-to-ULV transition takes place at a temperature corresponding to the long-chain lipid's gel-liquid crystalline transition, implying that increased miscibility levels between the long- and short-chain lipids allows the short-chain lipid to diffuse from the disc's edge, causing the line tension to increase and the modulus of rigidity to decrease. This series of events gives rise to the formation of monodisperse ULVs.[6] These ULVs are stable over extended periods of time, namely, weeks,[1] and are thus considered to be good candidates as drug carriers.

In our previous studies of long- and short-chain lipids, both lipid species were disaturated zwitterionic phospholipids, which were doped with small amounts of an acidic long-chain lipid, namely, dimyristoyl phosphatidylglycerol (DMPG). Here, we investigate the morphology of a mixture composed of dipalmitoyl and dihexanoyl phosphatidylcholine (DPPC and DHPC, respectively) and the acidic lipid dioleoyl phosphatidylserine (DOPS). This particular combination of lipids was chosen to optimize the interactions between Saposin C (Sap C)—a glucosyl protein

necessary for the hydrolysis function of glucosylceramidasein lysosomes[7]—and the acidic lipid aggregates (containing charged DOPS), while at the same time attempting to maximize the potential for stable ULV formation through the use of short- and long-chain lipids. In the absence of this function, glucosylceramide accumulates in the brain, leading to Gaucher disease.[8] Another disease resulting from the accumulation of glycosphingolipids (GSL) is metachromatic leukodystrophy, which may also be caused by deficiencies of lysosomal enzyme and saposin activators.[9,10] As well as its specific role in enzymatic activation,[11-13] SapC is also capable of neuritogenic activity,[13-18] intermembrane transport of gangliosides and GSL,[19] lipid antigen presentation,[20-22] and membrane-fusion induction activities.[23-25] It should be noted that the intravenous administration of SapC

* Corresponding author. Tel.: 613-584-8811, ext. 6380. Fax: 613-584-4040. E-mail: mu-ping.nieh@nrc.gc.ca.

† National Research Council at Canada.

‡ Guelph-Waterloo Physics Institute and Biophysics Interdepartmental Group.

§ Cincinnati Children Hospital Medical Center and University of Cincinnati College of Medicine.

(1) Nieh, M.-P.; Harroun, T. A.; Raghunathan, V. A.; Glinka, C. J.; Katsaras, J. *Biophys. J.* **2004,** *86,* 2615–2629.

(2) Egelhaaf, S. U.; Schurtenberger, P. *Phys. Rev. Lett.* **1999,** *82,* 2804–2807.

(3) Nieh, M.-P.; Raghunathan, V. A.; Kline, S. R.; Harroun, T. A.; Huang, C.-Y.; Pencer, J.; Katsaras, J. *Langmuir* **2005,** *21,* 6656–6661.

(4) Nieh, M.-P.; Harroun, T. A.; Raghunathan, V. A.; Glinka, C. J.; Katsaras, J. *Phys. Rev. Lett.* **2003,** *91,* 158105.

(5) Lesieur, P.; Kiselev, M. A.; Barsukov, L. I.; Lombardo, D. *J. Appl. Crystallogr.* **2000,** *33,* 623–627.

(6) Fromherz, P. *Chem. Phys. Lett.* **1983,** *94,* 259–266.

(7) Beutler, E. *PLoS Med.* **2004,** *1,* 118–121.

(8) Pàmpols, T.; Pineda, M.; Girós, M. L.; Ferrer, I.; Cusi, V.; Chabás, A.; Sammarti, F. X.; Vanier, M. T.; Christomanou, H. *Acta Neuropatol.* **1999,** *97,* 91–97.

(9) Zhang, X. L.; Rafi, M. A.; DeGala, G.; Wenger, D. A. *Proc. Natl. Acad. Sci. U.S.A.* **1990,** *87,* 1426–1430.

(10) Schnabel, D.; Schroder, M.; Sandhoff, K. *FEBS Lett.* **1991,** *284,* 57–59.

(11) Sandhoff, K.; Kolter, T.; Harzer, K. In *The Metabolic and Molecular Bases of Inherited Disease*; Scriver, C. R., Beaudet, A. L., Sly, W. S., Valle, D., Eds.; McGraw-Hill: New York, 2000; pp 3371–3388.

(12) Schuette, C. G.; Pierstorff, B.; Huettler, S.; Sandhoff, K. *Glycobiology* **2001,** *11,* 81R–90R.

(13) Qi, X.; Qin, W.; Sun, Y.; Kondoh, K.; Grabowski, G. A. *J. Biol. Chem.* **1996,** *271,* 6874–6880.

(14) Qi, X.; Kondoh, K.; Krusling, D.; Kelso, G. J.; Leonova, T.; Grabowski, G. A. *Biochemistry* **1999,** *38,* 6284–6291.

(15) O'Brien, J. S.; Carson, G. S.; Seo, H. C.; Hiraiwa, M.; Kishimoto, Y. *Proc. Natl. Acad. Sci. U.S.A.* **1994,** *91,* 9593–9596.

(16) Kotani, Y.; Matsuda, S.; Sakanaka, M.; Kondoh, K.; Ueno, S.; Sano, A. *J. Neurochem.* **1996,** *66,* 2019–2025.

(17) Kotani, Y.; Matsuda, S.; Wen, T. C.; Sakanaka, M.; Tanaka, J.; Maeda, N.; Kondoh, K.; Ueno, S.; Sano, A. *J. Neurochem.* **1996,** *66,* 2197–2200.

(18) Tsuboi, K.; Hiraiwa, M.; O'Brien, J. S. *Brain Res. Dev. Brain Res.* **1998,** *110,* 249–255.

(19) Hiraiwa, M.; Soeda, S.; Kishimoto, Y.; O'Brien, J. S. *Proc. Natl. Acad. Sci. U.S.A.* **1992,** *89,* 11254–11258.

(20) Zhou, D.; Cantu, C.; Sagiv, Y., 3rd; Schrantz, N.; Kulkarni, A. B.; Qi, X.; Mahuran, D. J.; Morales, C. R.; Grabowski, G. A.; Benlagha, K.; et al. *Science* **2004,** *303,* 523–527.

(21) Kang, S. J.; Cresswell, P. *Nat. Immunol.* **2004,** *5,* 175–181.

(22) Winau, F.; Schwierzeck, V.; Hurwitz, R.; Remmel, N.; Sieling, P. A.; Modlin, R. L.; Porcelli, S. A.; Brinkmann, V.; Sugita, M.; Sandhoff, K.; et al. *Nat. Immunol.* **2004,** *5,* 169–174.

(23) Wang, Y.; Grabowski, G. A.; Qi, X. *Arch. Biochem. Biophys.* **2003,** *415,* 43–53.

(24) Qi, X.; Chu, Z. *Arch. Biochem. Biophys.* **2004,** *424,* 210–218.

**Figure 1.** Amino acid sequence of human SapC and its functional domains. The six cysteines (bold-faced) and the *N*-glycosylation consensus sequence (*) are indicated. The two helical domains, H1 (YCEVCEFLVKEVTKLID) and H2 (EKEILDAFDKMCSKLPK), are highlighted in green and yellow, respectively. The abbreviations MBD and FD stand for membrane binding and fusogenic domain, respectively.

bound to PS ULV has also been used to demonstrate the ability to transport fluorescent labeled phospholipids into the central nervous system.[26] It therefore seems that the combined SapC−PS complex may lend itself to a new drug and gene delivery system specific to the treatment of neurological and brain diseases.

The functional domains of human SapC are shown in Figure 1. A fusogenic domain is located in the amino-terminal half of the SapC molecule, which includes the H1 and H2 peptides. Previously, the effects of SapC and its two helical domain peptides, H1 and H2, on the destabilization and restructuring of lipid membranes have been examined with atomic force microscopy (AFM).[27] AFM indicates that SapC can destabilize and restructure the acidic membrane to form thicker "patches" on the surface, eventually leading to the dissolution of the bilayer. However, neither H1 nor H2 alone have significant influence on membrane structure. H2 tends to interact with lipids where membrane defects are present, and then aggregates into rodlike structures. Membrane destabilization, as a result of SapC, also begins at defects, suggesting that the high-curvature defects promote membrane destabilization. While AFM results show the influence of SapC and its H1 and H2 segments on supported membranes, the potential influence of these proteins on vesicle stability and morphology are not known. Since the ultimate goal of this work is to design SapC-liposome complexes, it is important to characterize their stability and morphologies in solution. Here, we use SANS to characterize vesicles in the absence and presence of SapC, H1, and H2. This technique is capable of revealing both mesoscopic structural information related to vesicle size, shape and polydispersity, and nanoscopic information related to membrane thickness.

As a necessary first step in developing SapC−ULV complexes, we characterize the effect of composition on the DOPS/DPPC/DHPC ULV system, a system suitable for the study of SapC−membrane interactions. In particular, we determine the aggregate morphologies of this lipid mixture via dynamic light scattering (DLS), transmission electron microscopy (TEM), and SANS measurements. SANS is then used to characterize the influence of H1, H2, and SapC on these ULVs. For aggregates in the absence of peptides, DLS and TEM results confirm the presence of a bimodal population of ULVs with diameters of the order of ∼200 and >500 nm, consistent with fits to SANS data using a combination of form factors for oblate ellipsoidal vesicles and triaxial ellipsoidal shells. SANS data reveal that SapC promotes the aggregation of ULVs at high concentrations (62.5 $\mu$M) while at lower concentrations (6.25 $\mu$M), the ULV structure is unperturbed. Both H1 and H2 induce small decreases to the membrane thickness. While the H1 peptide does not appear to modify ULV size, or their size distribution, H2 shifts the equilibrium between the two ULV aggregates present. Qualitatively, these results are consistent with previous AFM findings.

## Materials and Methods

DOPS, DPPC, and DHPC were purchased in powder form from Avanti Polar Lipids (Alabaster, AL) and used without further purification. For DLS measurements, the [DOPS]:[DPPC] molar ratio ranges from 1:1 to 10:1 with ([DPPC] + [DOPS])/[DHPC] = 4 for all samples. Lipid mixtures were dissolved in filtered, ultrapure $H_2O$ (Millipore EASYpure UV) at a total lipid concentration of 10 wt % using a combination of vortexing and temperature cycling, between 4 and 50 °C. The homogenized 10 wt % solutions were then progressively diluted into 5, 2, 1, 0.5, and 0.1 wt % samples.

Prior to DLS measurements, the 0.1 wt % stock lipid samples were diluted 5-, 50-, and 200-fold and analyzed using an $N4^+$ particle sizer (Coulter, Miami, FL). It was determined that diluting the system had no effect on the size of the particles. For SANS experiments, the same sample preparation protocol was applied to the [DOPS]/[DPPC] = 10 sample except that $D_2O$ (99.9%, Chalk River Laboratories, Chalk River, ON), instead of $H_2O$, was used to obtain a sample with a total lipid concentration of 0.5 wt %. The 0.5 wt % sample was then further diluted into 0.1 and 0.05 wt % mixtures using an acidic buffer composed of equal volumes of 0.1 N sodium acetate (NaAc) and 0.1 N acetic acid (HAc). The resultant solution had a pH value of 4.78 ± 0.02 in $D_2O$ and was stable over a 12-fold dilution with $D_2O$.

SapC was overexpressed in *E. coli* cells using the IPTG-inducing pET system,[28] and His-tag proteins were eluted from nickel columns. After dialysis, the proteins were further purified by HPLC chromatography as follows: The C4 reverse phase column was equilibrated with 0.1% trifluoroacetic acid (TFA) for 10 min, and then the proteins were eluted in a linear (0−100%) gradient of 0.1% TFA in acetonitrile over 60 min. The major protein peak was collected and lyophilized, while protein concentrations were determined as described previously.[28] H1 (YCEVCEFLVKEVTKLID) and H2 (EKEILDAFDKMCSKLPK) peptides were synthesized by SynPep Corp. (California, USA) and dissolved in $D_2O$ at a concentration of 1.5 mg/mL. The 0.1 wt % lipid solution with [DOPS]/[DPPC] = 10 and ([DPPC] + [DOPS])/[DHPC] = 4 was then added to the two peptide solutions (1.5 mg/mL) at a volume ratio of 12:1, and the SapC solution at a volume ratio of 1:1, yielding a final peptide (or SapC) concentration of 62.5 $\mu$M (molar ratio of [lipid]/[SapC] = 22/1), a concentration higher than the SapC required to induce membrane destabilization.[23] For comparison purposes, a sample containing only 6.25 $\mu$M of SapC ([lipid]/[SapC] = 220/1) was also prepared.

SANS experiments were carried out on the 30 m NG7 SANS instrument located at the National Institute of Standards and Technology (NIST) Center for Neutron Research (NCNR, Gaithersburg, MD). First, 8.09 Å wavelength ($\lambda$) neutrons, a neutron focusing lens, and a long sample-to-detector distance (SDD = 15.3 m) were used to reach the lowest scattering vectors [$q = 4\pi/\lambda \cdot \sin(\theta/2)$, where $\theta$ is the scattering angle]. Two other SDDs (5 and 1 m) were also used, covering a combined $q$ range from 0.002 to 0.35 Å$^{-1}$ for all three SDDs. Raw 2-D data were corrected for detector sensitivity, background, empty cell scattering and sample transmission. The corrected data were then circularly averaged, around the beam center, yielding the customary 1-D data. These data were then put on an absolute intensity scale using the known incident beam flux. The incoherent plateau was determined by averaging the

(25) Liu, A.; Wenzel, N.; Qi, X. *Arch. Biochem. Biophys.* **2005**, *443*, 101−112.

(26) Chu, Z.; Sun, Y.; Kuan, C. Y.; Grabowski, G. A.; Qi, X. *Ann. N.Y. Acad. Sci.* **2005**, *1053*, 237−246.

(27) You, H. X.; Qi, X.; Grabowski, G. A.; Yu, L. *Biophys. J.* **2003**, *84*, 2043−2057.

(28) Qi, X.; Leonova, T.; Grabowski, G. A. *J. Biol. Chem.* **1994**, *269*, 16746−16753.

**Table 1. Hydrodynamic Radii (nm) from DLS Data of DOPS/ DPPC/DHPC Aggregates in Solution, Where ([DOPS] + [DPPC])/DHPC = 4[a]**

| DOPS/DPPC ratio | duration (days) | $R_H$, nm (%) | | |
|---|---|---|---|---|
| | | 1−100 | 100−200 | 400−800 |
| 1 | 1 | 40 (79) | 145 (12) | 441 (9) |
| 1 | 40 | 42 (76) | 173 (7) | 705 (17) |
| 5 | 1 | 29 (78) | 157 (11) | 570 (11) |
| 5 | 40 | none | 147 (51) | 689 (49) |
| 10 | 1 | none | 138 (70) | 582 (30) |
| 10 | 40 | none | 178 (56) | 746 (44) |
| 10 | 240 | none | 161 (49) | 452 (51) |
| 10 | 365 | none | 159 (51) | 471 (49) |

[a] Only the sample with DOPS/DPPC = 10 shows a bimodal distribution. Brackets indicate the percent population of each aggregate.

intensity of 10−20 high $q$ data points, and was then subtracted from the reduced data.

ULV size was determined by photon correlation spectroscopy[23,24] using an N4+ sub-micrometer particle size analyzer (Coulter, Miami, FL). Large vesicles were found to be polydisperse with diameters between 20 and 800 nm. The data were acquired at an angle of 90° and analyzed using a size distribution process (SDP) with an autocorrelation function. ANOVA analysis was used to determine statistical significance, while error bars denote the standard deviation.

TEM images were taken with an Hitachi TEM (H-7600, Hitachi, Japan) operated at an acceleration voltage of 80 kV. A droplet of each sample was placed on a nickel grid coated with a support Formvar film (200 mesh, a thickness range from 30 to 75 nm, Electron Microscopy Sciences, PA). The grid was placed on filter paper at room temperature for 2 h. Prior to TEM analysis, the background was optimized at high magnification, while the area of interest was located at low magnification (50−1000×). A single vesicle could be viewed up to 50000× magnification. TEM micrographs were taken using a dual AMT CCD digital camera (2 × 2 K, 16 bit) with appropriate image acquisition software.

## Results

Motivated by the results of Wang et al.,[23] who discovered that SapC only functions in the presence of negatively charged unsaturated lipids (i.e., DOPS) at acidic conditions, the present system is composed mainly of DOPS and lesser amounts of DPPC and DHPC. DLS results of the various [DOPS]/[DPPC] molar ratio samples (Table 1) indicate that only the [DOPS]/ [DPPC] = 10 sample exhibits a bimodal size distribution, while the remaining samples contain at least three populations. For this reason, only the [DOPS]/[DPPC] = 10 sample was used to further investigate the effects of SapC, H1, and H2 on the structure of these ULVs. DLS data also show that DOPS/DPPC/DHPC samples are stable over a period of 12 months (Table 1). This is evidence that the addition of DPPC and DHPC dramatically enhances, compared to sonicated DOPS, the stability of these aggregates and offers the possibility that they can be used in practical applications. Note that the apparent sizes, or hydro-dynamic radii of ULVs, as calculated from DLS results are based on the assumption that the ULVs are spherical. For prolate and oblate vesicles an accurate determination of the vesicle axial ratio requires the measurement of both the vesicle's hydrodynamic radius and the radius of gyration obtained using DLS and static light scattering (SLS), respectively.[29] For nonspherical vesicles, calculations of ULV mass, or surface area, from using the hydrodynamic radius can be off by as much as 10%.

(29) Pencer, J.; Hallett, F. R. *Langmuir* **2003**, *19*, 7488−7497.
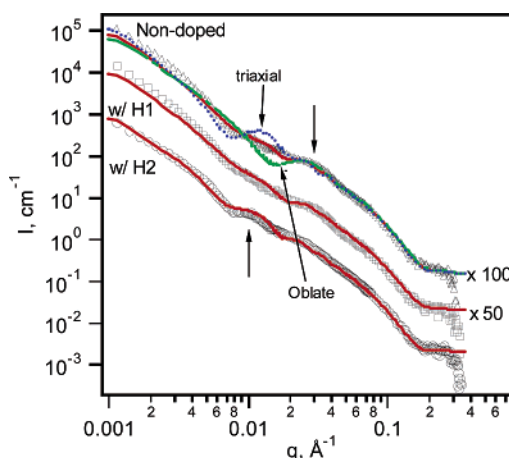


**Figure 2.** SANS data of 0.1% DOPS/DPPC/DHPC (triangles), H1-doped (squares), and H2-doped (circles) mixtures. Solid lines represent best fits to the data. The two broad peaks, indicated by arrows, are the result of correlation lengths present in the system. The blue (dots) and green (dashes) lines are, respectively, the results of the triaxial ellipsoidal and oblate shell models used to fit the 0.1% nondoped system.

Figure 2 shows SANS data of the 0.1 wt % lipid mixture ([DOPS]/[DPPC] = 10) and the H1- and H2-doped lipid mixtures in acetate $D_2O$ buffer. Lower levels of SapC (6.25 $\mu$M) do not appear to perturb the size of ULVs or their membrane structure (the same as nondoped mixtures). In the case of high SapC levels (62.5 $\mu$M), the SapC-doped lipid system forms large aggregates that precipitate out of solution (not amenable for SANS), an observation consistent with previous studies, indicating that SapC destabilizes membranes.[23] As a result, we only focus on the effects of H1 and H2 on the structure of ULV. The scattering curves of the non-SapC-doped samples (Figure 2) share a common feature in that they contain two broad peaks centered along $q \sim$ 0.01 and 0.03 $Å^{-1}$, indicative of the presence of two correlation lengths in the system. To better understand the origins of these peaks, a 0.05 wt % pure lipid mixture was also examined. SANS data of the 0.05 wt % sample (not shown) can be scaled to overlap the 0.1 wt % sample data, indicating that the two broad peaks are inherent to the aggregate morphologies and not the result of interparticle interactions.

For $q > 0.06\ Å^{-1}$ the differences in intensity among the three data sets (Figure 2) are indistinguishable. Analysis of a modified Guinier plot[30] (also known as Kratky-Porod plot) applied to all three samples, where $\ln(I \cdot q^2)$ has a linear relationship with $q^2$ in the range between $5 \times 10^{-3}$ and $2.5 \times 10^{-2}\ Å^{-2}$ (Figure 3), indicates the existence of a lamellar structure. The bilayer thickness is then derived from the square root of the slope multiplied by $\sqrt{12}$.

The best-fit results show that the nondoped mixture forms the thickest bilayer ($37.7 \pm 0.7$) Å, while the H1- and H2-doped bilayers are slightly thinner ($35.8 \pm 0.8$ and $36.2 \pm 0.6$ Å, respectively).

For $q \le 0.06\ Å^{-1}$, the scattering curve of the H1-doped system, compared to the H2-doped system, is similar to that of the nondoped lipid mixtures, implying that no significant change is taking place in the aggregate morphology upon doping the membranes with H1 peptide. This observation is also consistent with a previous AFM report,[27] where H1 was found to have no effect on 1-palmitoyl-2-oleoyl phosphatidylserine (POPS) bi-layers. In the case of H2-doped SANS data, qualitative differences

(30) Porod, G. In *Small Angle X-Ray Scattering*; Glatter, O., Kratky, O., Eds.; Academic Press: New York, 1982; Chapter 2, p 36.
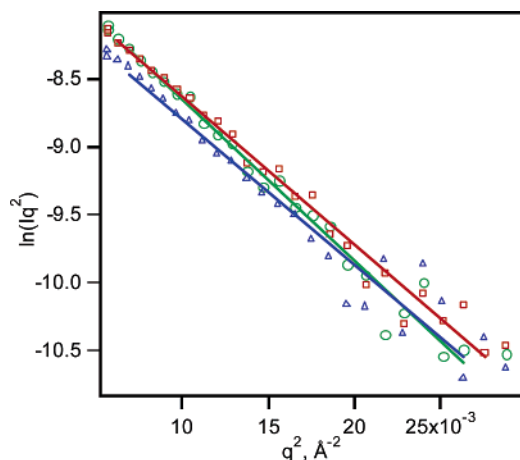
**Figure 3.** Modified Guinier plot for the 0.1 wt % DOPS/DPPC/DHPC mixture (green circles), H1-doped system (blue triangles), and H2-doped (red squares) systems. Lines represent the best fits to the data.
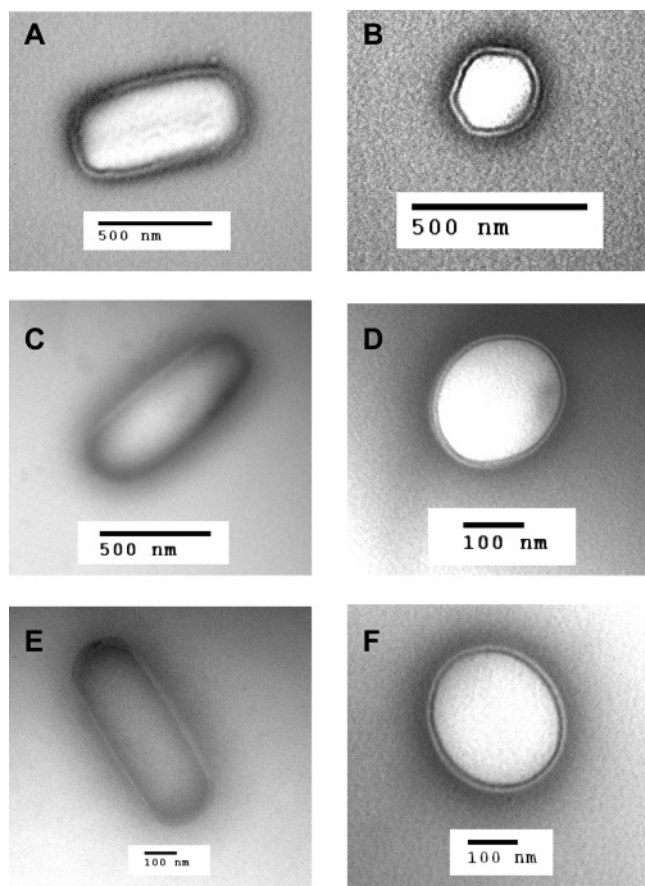


**Figure 4.** Representative TEM images of a DOPS/DPPC/DHPC mixture (A and B) and H1-doped (C and D) and H2-doped (E and F) mixtures. The triaxial ellipsoidal vesicles, i.e., A, C, and E, are all of similar size (projected cross-sectional area 150–200 nm × 600–800 nm). So are the oblate vesicles with projected radii around 100–150 nm. These dimensions are consistent with the best-fit results of the SANS data (see Appendix).

from those of the pure lipid mixture are observed in the slope of the low-$q$ region ($q < 0.003$ Å$^{-1}$) data, and the width and intensities of the two peaks.

TEM images of all three samples were obtained (Figure 4) and particles with two populations of morphologies were observed. One morphology has a circular 2-D projection with a radius ~150–200 nm, while the other morphology has an

elongated ellipsoidal projection with long and short axes of dimensions between 600 and 800 nm, and 100 and 200 nm, respectively. This result is consistent with the DLS data; however, the bimodal distribution can either be a mixture of spherical and ellipsoidal vesicles or of oblate and triaxial ellipsoidal vesicles, depending on the thickness of the particles along the axis perpendicular to the projection. Since the former distribution (e.g., mixture of spherical and ellipsoidal vesicles) does not adequately fit the data, we formulated a model which includes oblate and triaxial ellipsoidal ULVs (see Appendix). The oblate morphology has two equal-length major axes and one polydisperse minor axis (shown in Figures 4B, 4D, 4F), while the triaxial ellipsoid morphology has three unequal length axes (Figures 4A, 4C, 4E). This model requires eight fitting parameters, namely, three axes for the triaxial ellipsoidal shell, two axes for the oblate shell, polydispersity of the shorter axis for the oblate morphology, the bilayer thickness, and the population ratio of triaxial-to-oblate. However, results from TEM and DLS measurements, as well as the Kratky-Porod analysis, allows us to constrain the bilayer thickness and the lengths of the two major axes in the case of the oblate shell, and the two longer axes for the triaxial ellipsoidal shell. This leaves the lengths of the shorter axes, the polydispersity of the shorter axis of the oblate shell and the population ratio of triaxial-to-oblate as free fitting parameters. The best-fit result shows that the oblate and triaxial ellipsoids have a bilayer thickness of 40 ± 5 Å, slightly larger than the result obtained from the modified Guinier plot. The shortest axis of the triaxial ellipsoid and minor axis of the oblate morphologies are 250 ± 20 and 100 ± 10 Å, respectively. These features give rise to the broad peaks (~0.01 and ~0.03 Å$^{-1}$) in the SANS data. Moreover, the best-fit data for the lengths of the major axis of the oblate (~150 nm) and the two longer axes of the ellipsoid (~200 and 500 nm) morphologies are consistent with the TEM results shown in Figure 4. The percent population of oblate ellipsoids is found to be ~40 ± 10% in the case of the H2-doped mixture, while it is ~60 ± 10% for the non- and H1-doped mixtures. The higher intensity of the first peak (~0.01 Å$^{-1}$) observed in the H2-doped system indicates a higher population of triaxial ellipsoidal vesicles, consistent with the best-fit result. It therefore seems that the H2 peptide favors the formation of triaxial ellipsoidal vesicles. In summary, all three techniques point to the presence of two morphologies, namely, triaxial and oblate ellipsoids.

## Discussion

While our primary goal in studying DPPC/DHPC/DOPS mixtures was to find an appropriate ULV system to study SapC−membrane interactions, our observation of the unexpected behavior of this lipid mixture merits further discussion. Based on our previous experimental results,[3] our initial expectations were to find appropriate conditions for the formation of monodisperse, spherical ULVs. However, as noted above, we find that while DPPC/DHPC/DOPS do form ULVs, the size distributions of the mixtures examined by DLS were multimodal. In the case of bimodally distributed ULVs, we find that each population has a nonspherical shape and a narrow size distribution. This observation leads us to speculate that the mechanism for present ULV formation is different from that taking place in DMPC/DHPC/DMPG mixtures.[3]

In previous studies, we found that the formation of low-polydispersity ULVs required heating the system from the low-temperature bilayered micelle (bicelles) morphology. ULV size was found to be dependent on the size of the bicelles and was most likely modulated by such factors as the rim line tension

energy, the bilayer's bending rigidity, and the rate of bicelle coalescence. Moreover, the DMPC/DHPC/DMPG bicelle → ULV transition was closely associated with the gel → liquid crystalline transition of DMPC, which takes place at ∼23 °C. If DPPC/DHPC/DOPS were to exhibit a similar behavior, it is likely that the bicellar morphology would be found near or below −11 °C, the temperature where DOPS' fatty acid chains undergo a melting transition. Since dilution of DMPC/DHPC/DMPG mixtures, at high temperatures, led to the formation of ULVs with a broad size distribution,[3] we conclude that the ULV formation mechanism taking place here is different from that previously investigated.

Demé et al. reported that, upon dilution and as a result of collective membrane fluctuations, pure DOPS lamellar stacks completely unbind, forming *polydisperse* ULVs.[31,32] Thus, although pure DOPS suspensions can also form ULVs, we can dismiss this as the mechanism of formation taking place here. We speculate that the nonspherical ULVs observed are stabilized by having the short-chain DHPC populating the high curvature region of the ULV, while the long-chain DPPC provides the requisite rigidity needed for stable bilayers. However, this does not explain the low aggregate polydispersity, and a more detailed study is needed to better understand the formation mechanism of the oblate and triaxial ellipsoidal ULVs.

It is unusual that although we observe a bimodal ULV size distribution, the polydispersities of the individual populations are reasonably low. It may be that these two populations represent equilibrium, minimum energy states which may exchange material freely, or it could be that the individual ULVs are dynamic structures capable of switching back and forth between these two morphologies. The notion that morphologies freely transform has been predicted theoretically[33,34] and may also be analogous to previous experimental observations where prolate free vesicles transformed into oblate vesicles, and vice versa.[29,35,36]

The ellipsoidal ULV morphology is also unexpected, but could be a consequence of membrane lateral heterogeneities. It has recently been shown by SANS that ternary mixtures containing saturated and unsaturated lipids can exhibit lateral segregation.[37] Furthermore, Bagatolli and Gratton[38] discovered, as a function of increasing temperature through the gel → liquid crystalline transition, a complicated spherical−polygonal−ellipsoidal transition in giant ULVs. The seemingly polygonal shape (Figure 4B) presumably resulted from the lateral phase separation between these two phases, where the DOPS and DHPC lipids are in the $L_\alpha$ phase, while DPPC is in the gel phase. In addition, due to the different lipid species possessing different hydrocarbon chain lengths, each domain may contribute to determining the length of each of the ellipsoid's axes. To the best of our knowledge, the formation of monodisperse, triaxial ellipsoidal, pure phospholipid vesicles has not been previously reported, although there are examples of spherical vesicles transforming into oblate or irregular-shaped vesicles induced by the polymerization of actin.[39,40] Here, we speculate that this may be the result of lateral phase separation within the membrane.

The best fits to the high $q$ data result in a bilayer thickness between 38 and 40 Å. Since the ellipsoidal shell model assumes a constant bilayer thickness along the prime axis, and a uniform scattering length density across the bilayer, the value for the bilayer thickness could be expected to be slightly greater than values obtained from more detailed models.[41] The modified Guinier plot indicates that compared to H1- and H2-doped ULVs, nondoped ULVs possess a thicker bilayer. This demonstrates that although H1 and H2 have a thinning effect on the bilayer, they do not destabilize the bilayer. Wang et al. have reported that H1 and H2 can inhibit SapC-induced membrane fusion, implying that they may possibly bind at the same DOPS site as SapC, thus reducing SapC's interaction with the membrane.[23] Their results also showed that H1 is more effective than H2 in the inhibition of membrane fusion. This is consistent with the fact that H1 has a greater effect on bilayer thinning.

A previous AFM study has shown that H2 formed patches on the membrane, which were inferred to be rodlike structures populating regions of bilayer defects.[27] SANS data indicate a population shift of particle morphologies from oblate to triaxial ULVs upon doping with H2, compared to non- and H1-doped ULVs. Since the short-chain DHPC is known to create defects in the membrane,[42,43] this lipid mixture may provide a suitable environment for H2 to associate with, leading to the preferred formation of triaxial ellipsoidal ULVs.

## Conclusions

Through the combined use of SANS, TEM, and DLS, we are able to characterize the various morphologies assumed by mixtures of DOPS/DPPC/DHPC. Two low-polydispersity morphologies are observed, namely, oblate and triaxial ellipsoidal ULVs. Here, the ULV formation mechanism seems to differ from that reported previously[1,3,5,31,32] and demonstrates that low-polydispersity ULVs can be formed even in the absence of the long-chain lipid undergoing a gel → liquid crystalline transition. SANS results show that H1 and H2 do not destabilize the bilayer morphology, a result consistent with previous AFM data,[27] but that H1 has a greater effect on bilayer thinning. Moreover, the addition of the H2 peptide does increase the ratio of triaxial-to-oblate ellipsoidal vesicles, presumably due to a change in miscibilities of the various lipid components. On the other hand, the addition of SapC destabilizes the membrane and results in the precipitation, from solution, of large aggregates.

Increasing evidence suggests that liposomal vesicles are effective carriers for a variety of therapeutics.[44] However, the efficacy of a particular system in treating disease and its commercial viability are of prime importance. In this report, PS containing ULVs have been shown to form spontaneously, are highly stable, and have low polydispersity. Here, we provide a protocol potentially for the scaled-up industrial production of SapC-bound ULVs. The results of this study will facilitate the development of SapC−PS ULV complexes which can then be tested for the in vivo transport of therapeutic agents.

(31) Demé, B.; Dubois, M.; Gulik-Krzywicki, T.; Zemb, T. *Langmuir* **2002**, *18*, 997−1004.
(32) Demé, B.; Dubois, M.; Zemb, T. *Langmuir* **2002**, *18*, 1005−1013.
(33) Miao, L.; Seifert, U.; Wortis, M.; Döbereiner, H.-G. *Phys. Rev. E* **1994**, *49*, 5389−5406.
(34) Döbereiner, H.-G.; Evans, E.; Kraus, M.; Seifert, U.; Wortis, M. *Phys. Rev. E* **1997**, *55*, 4458−4474.
(35) Döbereiner, H.-G.; Seifert, U. *Europhys. Lett.* **1996**, *36*, 325−330.
(36) Xu, L.; Döbereiner, H.-G. *J. Biol. Phys.* **1999**, *25*, 35−39.
(37) Pencer, J.; Mills, T.; Anghel, V. N. P.; Krueger, S.; Epand, R. M.; Katsaras, J. *Eur. Phys. J. E* **2005**, *18*, 447−458.
(38) Bagatolli, L. A.; Gratton, E. *Biophys. J.* **1999**, *77*, 2090−2101.
(39) Palmer, A. F.; Wingert, P.; Nickels J. *Biophys. J.* **2003**, *85*, 1233−1247.
(40) Li, S.; Palmer, A. F. *Langmuir* **2004**, *20*, 4629−4639.

(41) Kučerka, N.; Nagle, J. F.; Feller, S. E.; Balgavy, P. *Phys. Rev. E* **2004**, *69*, 051903.
(42) Nieh, M.-P.; Glinka, C. J.; Krueger, S.; Prosser, S.; Katsaras, J. *Langmuir* **2001**, *17*, 2629−2638.
(43) Nieh, M.-P.; Glinka C. J.; Krueger, S.; Prosser, R. S.; Katsaras, J. *Biophys. J.* **2002**, *82*, 2487−2498.
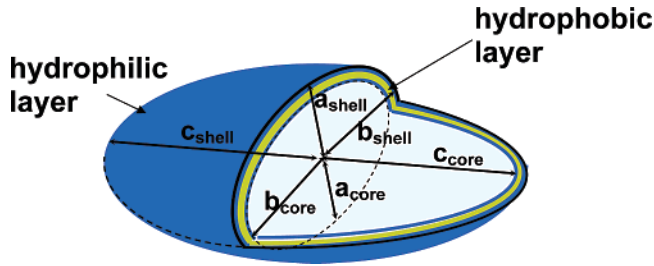(44) Allen, T. M.; Cullis, P. R. *Science* **2004**, *303*, 1818−1822.

**Figure 5.** Proposed model for a unilamellar, triaxial ellipsoidal bilayered vesicle. The hydrophilic (headgroups) and hydrophobic (hydrocarbon tails) regions are shown in blue and yellow, respectively. In the case of oblate vesicles, b and c are equal.

## Appendix

The model for a unilamellar triaxial ellipsoidal vesicle is depicted as an ellipsoidal shell (Figure 5) with different core lengths along the three prime axes, $a_{core}$, $b_{core}$, and $c_{core}$ ($a_{core} \leq b_{core} \leq c_{core}$). The shell lengths along the axes $a_{shell}$, $b_{shell}$, and $c_{shell}$ are defined as $(a_{core} + l)$, $(b_{core} + l)$, and $(c_{core} + l)$, respectively, where $l$ is the bilayer thickness. Note that this approximation does not assume a constant bilayer thickness over the entire ULV along the bilayer normal direction. The form factor for a triaxial ellipsoidal shell averaged over all possible orientations, $P_{triax}(q)$, can thus be expressed as

$$P_{triax}(q) = \frac{1}{V_{triax}} \int_{-1}^{1} \int_{-1}^{1} A_{triax}(a_{core}, b_{core}, c_{core}, l, x, y, q)^2 \, dx \, dy$$
(A-1)

$$A_{triax}(q) = 3(\rho_{D_2O} - \rho_{lipid}) \left[ \frac{V_{total} j_1(u_{shell})}{u_{shell}} - \frac{V_{core} j_1(u_{core})}{u_{core}} \right]$$
(A-2)

where $j_1$ is the first-order spherical Bessel function,

$$j_1(x) = \frac{\sin x}{x^2} - \frac{\cos x}{x}$$

$u_i$ is defined as

$$q\sqrt{a_i^2 \cos^2\left(\frac{\pi x}{2}\right) + b_i^2 \sin^2\left(\frac{\pi x}{2}\right)(1 - y^2) + c_i^2 y^2}$$

($i$ represents shell or core), and $V_{total}$ and $V_{core}$ are the total and core volumes of the ellipsoid, respectively. $\rho_{D_2O}$ and $\rho_{lipid}$ denote the scattering length densities of $D_2O$ and lipid.

For oblate ellipsoidal vesicles, the form factor $P_{oblate}(q)$ can be obtained by letting $c_{core} = b_{core}$. Thus, $u_i$ becomes

$$q\sqrt{a_i^2 \cos^2\left(\frac{\pi x}{2}\right) + b_i^2 \sin^2\left(\frac{\pi x}{2}\right)}$$

Moreover, the Schultz function, $f(a)$, is employed to describe the distribution of the shorter axis (i.e., $a_{core}$) as shown below,

$$f(a) = \frac{p^{-2/p^2}}{\langle a \rangle \Gamma(1/p^2)} \left(\frac{a}{\langle a \rangle}\right)^{(1-p2)/p2} \exp\left(-\frac{a}{p^2 \langle a \rangle}\right) \quad (A-3)$$

where $\langle a \rangle$ is the average of $a$. $p$ is the polydispersity and is defined as $\sigma/\langle a \rangle$, where $\sigma$ is the standard deviation of $a$. A reasonable value for $p$ is in the range of 0−1.[45] The Gamma function, $\Gamma(1/p^2)$, is used to normalize the integral of the Schultz function. Equation A-3 is put inside the inner integration of eq A-1, resulting in

$$P_{oblate}(q) = \frac{1}{V_{oblate}} \int_{-1}^{1} \int_{0}^{\infty} f(a_{core}) \cdot A_{oblate}$$

$$(a_{core}, b_{core}, l, x, q)^2 \, da_{core} \, dx \quad (A-4)$$

The total scattering intensity for noninteracting vesicles (oblate and triaxial ellipsoid) can then be written as

$$I(q) = (\Phi_{lip} - \Phi_{oblate})P_{triax}(q) + \Phi_{oblate}P_{oblate}(q) \quad (A-5)$$

where $\Phi_{lip}$ and $\Phi_{oblate}$ are the volume fractions of the total lipid and oblate shell in solution, respectively. The fitting procedure is written in IGOR, which has been revised from the data analysis package developed at NIST.

(45) Hayter, J. B. Determination of structure and dynamics of micellar solutions by neutron small angle scattering. In *Physics of amphiphiles-micelles, vesicles, and microemulsions*; Degiorgio, V., Corti, M., Eds.; Amsterdam, 1985; pp 60−93.